

Process-controlled Grading of the Young's Modulus of AlSi10Mg Components Using L-PBF

J. Geis*, J. Reichwein*, H. Merschroth†, E. Kirchner*, M. Weigold†

*Technical University of Darmstadt, Institute for Product Development and Machine Elements,
Germany, 64287 Darmstadt

† Technical University of Darmstadt, Institute of Production Management, Technology and Machine
Tools, Germany, 64287 Darmstadt

Abstract

Laser Powder Bed Fusion (L-PBF) increases freedom in the design of components and is therefore well suited for the manufacturing of complex geometries tailored to their function. In addition, it is possible to influence the microstructural characteristics of the components by varying the process parameters during the L-PBF process. This allows shifting the load from areas with high stresses to less heavily loaded areas in order to exploit the full potential of the material. For this purpose, the process window in which the Young's modulus of the material AlSi10Mg can be varied was investigated. Subsequently, test geometries were analyzed by finite element method with respect to their critical component areas and a design for grading the Young's modulus to distribute stress more uniformly was developed. These specimens were then manufactured and compared with components manufactured using homogeneous parameters.

Introduction

Additive manufacturing processes are an emerging technology and have recently been used more and more in the industrial environment. From being used to manufacture prototypes at early stages of development, more and more serial components are being manufactured [1]. Besides the use of polymers, especially laser powder bed fusion (L-PBF) is used increasingly for the processing of metals [2]. In industries such as automotive or aerospace, the focus is on the energy efficiency of products and therefore the additive manufacturing of geometrically highly complex, lightweight components is becoming progressively more important [3]. To ensure the quality of components, approaches are being developed in the research environment in which it is possible to predict the microstructure and fatigue life based on in-situ data generated during the manufacturing process. In addition, efforts are being made to adapt the process parameters directly on the basis of live data gathered from the process. [2]

At present, manufacturing with static process parameter sets can be regarded as the industry standard. In order to increase the surface quality, overhanging and upward facing component areas are manufactured with slightly deviating process parameters in these static parameter sets. Nevertheless, there is an anisotropy of the mechanical properties along the build direction due to the fact that the cooling rates are dependent on the component height and geometry and thus affect the resulting microstructure. The change in the cross-sectional area of a component along the build direction therefore has an enormous influence on heat transfer and can amplify the anisotropy effect. [4] For this reason, approaches are being developed to homogenize the cooling rate over the entire manufacturing process. The laser power is adjusted based on the components geometry and adjusted in such a way that a certain maximum temperature is not exceeded. [5, 6] The L-PBF process can achieve high cooling rates compared to casting

processes, for example, which means that the formation of fine microstructures can be achieved. Coarse grain structures, on the other hand, typically occur in areas of the component where heat transfer is relatively limited. [7, 8] By varying the process parameters during the manufacturing process, it is possible to influence the microstructure in order to adapt it to the desired functional performance [9]. This targeted adaptation of the microstructure has already been demonstrated with several examples: Popovich et al. produced components from Inconel 718 by using different exposure strategies and varying the process parameters, causing a direct transition from a fine to a coarse microstructure. This procedure resulted in a significant difference in the hardness of these two component areas by 20%. [10] Attard et al. investigated the influence of the process parameters on the microstructure and were able to adapt a turbine blade made of Inconel 718 to the present loads by adjusting the manufacturing strategy [11]. Parikh and Kuttolamadom were also able to show for the alloy 316L that a reliable variation of the mechanical properties is possible for the production of functional graded materials[9].

Based on the possibility of adapting the microstructure by adjusting the process strategy, the present work investigates the approach to what extent this is possible with the alloy AlSi10Mg. This material is widely used in the industry and is highly popular in lightweight applications. However, due to its brittle behavior, this material is particularly susceptible to notch effects, which cause abrupt failure of the component. Ductile materials, on the other hand, can reduce stress peaks by plastic flow. [12] Therefore, the following approach is to reduce the stresses at a critical location of the component by locally increasing the ductility by means of a process-related control. Stresses are then to be transferred to areas of the component that are less severely stressed in comparison. The Young's modulus is used as the design parameter, since it is a measure of the ductility of a material. Figure 1 schematically illustrates the intended grading of the Young's modulus with an analog by coil springs of different stiffness as well as the path of force lines. The increased ductility at the critical point has the effect of relieving it, since stresses are shifted to stiffer areas of the component, and this results in the local tensile strength not being reached until the overall load is higher. The load-bearing capacity of the entire component should thus be increased without adjusting the macro-geometry.

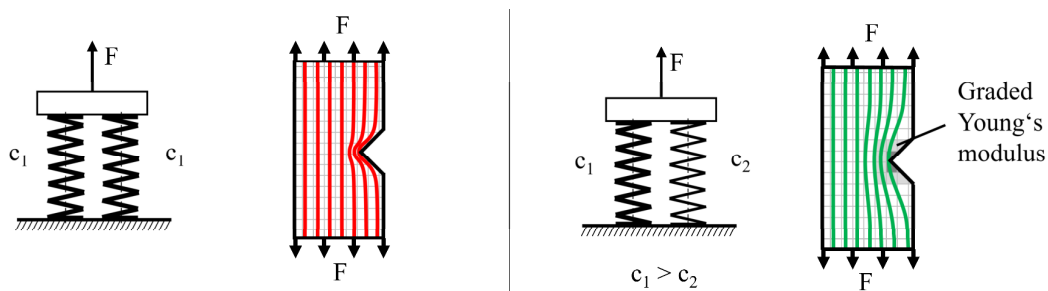


Figure 1: Principle concept of stress redistribution by grading the Young's modulus illustrated by an analog with differently stiff coil springs (based on [13])

Methodology and Analysis Methods

In this paper, a process window for the manufacturing of different Young's moduli is first determined using a full-factorial experimental design. For this purpose, the relative density of the manufactured samples is used to exclude individual process parameter sets that exceed a certain porosity. Subsequently, the mechanical properties are determined by means of tensile tests. Using the achievable Young's moduli, a design of a graded specimen with bore is carried out using a developed FE-based

grading tool. This graded specimen is then manufactured and compared with a homogeneous specimen. All specimens were manufactured with an EOS M290 using the material AISi10Mg with a layer height of 30 μm .

Preliminary investigations, which dealt with the limits of the process window, showed that the Young's modulus can be varied in the range of 46 to 62 GPa [13]. In the literature it was found that the variation of the parameters laser power, scan speed as well as hatch distance have a significant effect on the mechanical properties of the additively manufactured components [7]. In order to be able to manufacture components with Young's moduli within the determined limits, a full-factorial experimental design is being executed in which the aforementioned process parameters are varied. Table 1 lists the three factors evaluated with three gradations.

Table 1: Process parameters for execution of a full-factorial experimental design to determine the process window for variation of the Young's modulus

	low	middle	high
Laser power [W]	250	310	370
Hatch distance [mm]	0.07	0.13	0.19
Scan speed [mm/s]	1000	1500	2000

With the resulting 27 process parameter sets, three cubes each with dimensions of 10x10x10 mm³ are manufactured. The relative density of the specimens is then determined with the Kern ABT 220-4nm analytical scale using Archimedes' principle. All process parameter sets that can be used to produce specimens with a relative density < 99.5% will not be considered in the following. The porosity of these specimens has an unpredictable influence on their mechanical properties, since the inner pores lead to a wide distribution of these [14].

The remaining sets of parameters are now used to manufacture tensile specimens for determining the mechanical properties. Specimen shape A from DIN 50125 was selected for this purpose and the dimensions of this specimen shape are shown in Figure 2. In order to eliminate the notch effect of the rough surface of L-PBF manufactured specimens during the tensile tests, the specimens were manufactured with a slight oversize of 0.03 mm and brought to final contour by subtractive manufacturing processes. Three tensile specimens are manufactured and machined for each set of parameters investigated. The tensile tests were performed with a ZwickRoell Z100, and a deformation rate of 0.1%/s was selected by controlling the traverse path. The elongation of the tensile specimens was measured with a video extensometer. All tensile specimen were not heat treated before testing.

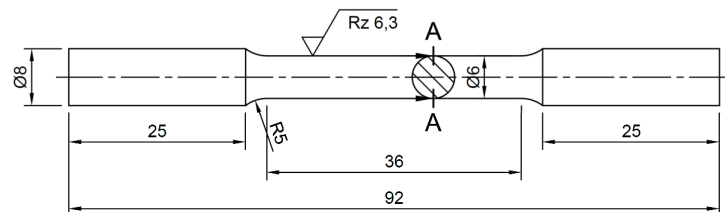


Figure 2: Dimensions in mm of tensile specimen shape A according to DIN 50125 for determining the material properties of the tested specimens

In order to be able to adapt the design of a component to the external load, the component is analyzed by means of finite element simulation and graded based on these results so that the critical location is relieved. The developed grading tool uses Abaqus via programming interface and works as follows. First, the range in which the Young's modulus can be varied must be defined and the component geometry divided into equally sized voxels. In the course of the gradation, these voxels are used to simultaneously assign new Young's moduli to the finite elements of different sizes within these voxels. After specifying the external loads as well as the boundary conditions, the stress state of the component is calculated with homogeneous material properties and the mesh size is iteratively refined at highly stressed locations. Gaussian points are then used to determine the average stresses in the voxels, on the basis of which the subsequent grading takes place. The Young's modulus of these voxels is iteratively adjusted to the existing stress state in successive finite element analyses according to the following concept in linearly distributed, discrete steps: The occurring stress range is first divided into two sections. The voxels, which are located in the lower section of the stress range, are provided with the highest Young's modulus in order to ensure the stiffest possible structure. The remaining voxels are assigned a Young's modulus in the achievable variation range in linear gradation according to the stress level present. Voxels with high stress are assigned a low modulus of elasticity and vice versa. If the occurring stresses cannot be reduced further by adjusting the Young's modulus, the termination criterion is fulfilled and the grading process is terminated. The assignment of the Young's moduli to the voxels obtained by the grading tool is used to define the process parameter sets during the later manufacturing process.

The specimens geometry investigated is a plate with a bore, the dimensions of which are given in figure 3a. Eight specimens each are manufactured with homogeneous as well as heterogeneous process parameters and subsequently examined with the ZwickRoell Z100 tensile machine. The specimens are manufactured with an oversize of 0.3 mm and then brought to its final dimensions using subtractive manufacturing processes to eliminate the notch effect of the rough surface. Under tensile loading of this geometry, a stress peak forms at the edges of the bore, as shown qualitatively in Figure 3b. The bore acts like a notch and can be described with a notch shape number of $\alpha_{zd} = 2,24$ under tensile loading. Thus, the stress peak at the notch is slightly more than twice the nominal stress at this location, which means that failure will occur in the center of the specimen. All tensile specimen were tested in "as-built" condition.

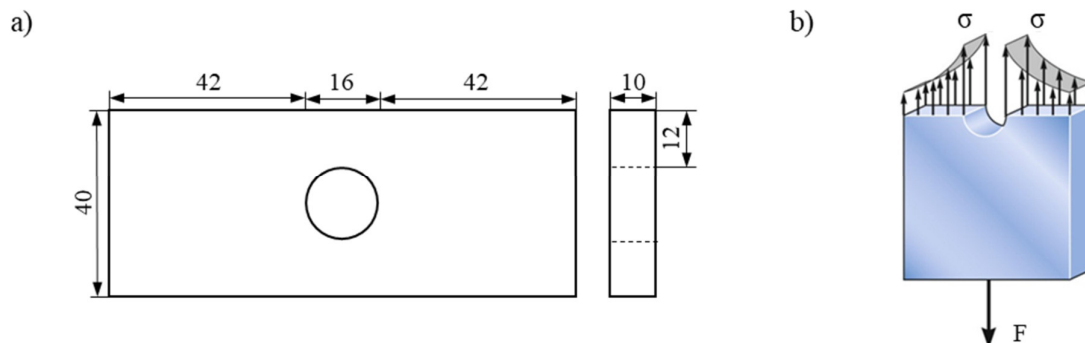


Figure 3: a) Dimensions in mm of the geometry of a specimen with a bore b) Qualitative illustration of the stress peaks during tensile loading of the specimen at the edges of the bore [15]

Results and Discussion

Figure 4 shows the results of the density measurement plotted against the volumetric energy density of the process parameter sets. The red line shows the defined limit of 99.5% relative density, above which the process parameter sets are further investigated in the following. The exact values can be found in table 2, the entries are sorted in ascending order of volumetric energy density. The reference value of the density measurement is taken from the powder manufacturer's data sheet and amounts to 2.67 g/cm³, therefore individual values are found which slightly exceed 100% relative density [16]. It can be clearly seen that parameter sets with volumetric energy densities of < 35 J/mm³ have a lower relative density and are therefore not considered further. This is due to insufficient energy to completely melt all powder particles. Since the limits of the process parameter variation have been determined by preliminary tests, as described previously, the number of parameter sets to be eliminated is comparatively low, at 5 out of 27.

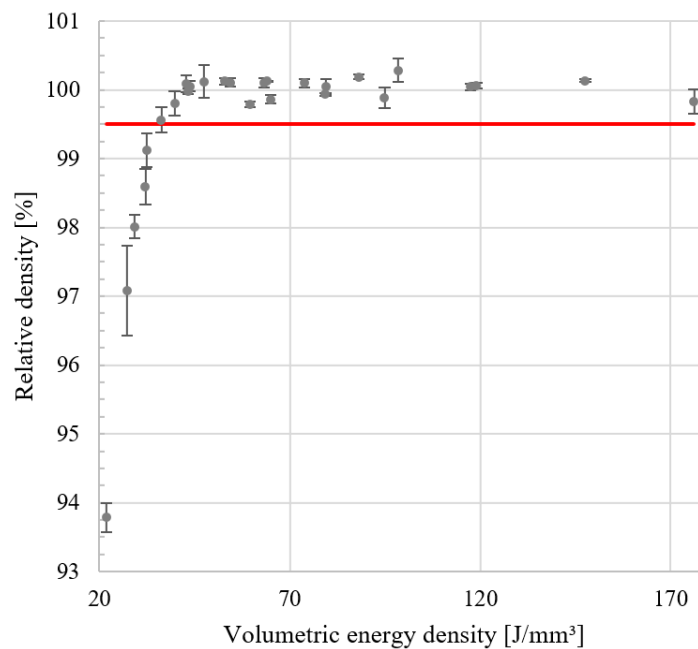


Figure 4: Volumetric energy density of the investigated parameter sets plotted against the relative density of the cube-shaped samples related to the density of the material data sheet of 2.67 g/mm³

Table 2: Process parameter sets with the associated volume energy density and the measured relative densities to the reference value of 2.67 g/cm³ from the material data sheet

Laser power [W]	Scan speed [mm/s]	Hatch distance [mm]	Volumetric energy density [J/mm ³]	Relative Density [%]
250	2000	0,19	21,93	93,79 ± 0,21
310	2000	0,19	27,19	97,08 ± 0,66
250	1500	0,19	29,24	98,01 ± 0,17
250	2000	0,13	32,05	98,59 ± 0,26
370	2000	0,19	32,46	99,12 ± 0,25
310	2000	0,13	39,74	99,80 ± 0,18
250	1500	0,13	42,74	100,09 ± 0,12
370	1500	0,19	43,27	99,98 ± 0,04
250	1000	0,19	43,86	100,05 ± 0,07
370	2000	0,13	47,44	100,12 ± 0,24
310	1500	0,13	52,99	100,13 ± 0,05
310	1000	0,19	54,39	100,10 ± 0,06
250	2000	0,07	59,52	99,79 ± 0,04
370	1500	0,13	63,25	100,10 ± 0,07
250	1000	0,13	64,10	100,12 ± 0,01
370	1000	0,19	64,91	99,86 ± 0,06
310	2000	0,07	73,81	100,10 ± 0,06
250	1500	0,07	79,37	99,93 ± 0,02
310	1000	0,13	79,49	100,05 ± 0,11
370	2000	0,07	88,10	100,19 ± 0,04
370	1000	0,13	94,87	99,88 ± 0,15
310	1500	0,07	98,41	100,28 ± 0,17
310	1500	0,19	100,27	99,56 ± 0,19
370	1500	0,07	117,46	100,04 ± 0,05
250	1000	0,07	119,05	100,06 ± 0,04
310	1000	0,07	147,62	100,13 ± 0,02
370	1000	0,07	176,19	99,83 ± 0,17

The tensile specimens were produced standing on the build platform with a support structure consisting of bulk material, whereby the orientation-dependent anisotropy of the mechanical properties was not initially considered. The aim of this paper is to clarify whether a gradation of the mechanical component properties is possible in principle by adapting the manufacturing process. However, consideration of anisotropy will need to be included in future work on this topic in order to exploit the full potential of this approach.

During the manufacturing of the standing tensile specimens, 8 process parameter sets tended to oversize the component geometry, resulting in collisions with the recoater of the additive manufacturing machine. These process parameter sets therefore had to be excluded from the following investigations in order to ensure process reliability during manufacturing. Thus, 14 of 27 process parameter sets were available for further investigation, which were examined in the tensile test with regard to their mechanical properties. In Figure 5, the process parameter sets are plotted in ascending order according to the measured Young's moduli, indicating the standard deviation, and numbered consecutively. The measured Young's moduli and the corresponding process parameter sets are shown in table 3. It can be seen that the limits of the variation range of the Young's modulus from the preliminary tests of 46 to 62 GPa could be achieved approximately. Furthermore, it has been possible to identify parameter sets that provide continuous coverage for grading the Young's modulus within these limits, as indicated by the plotted trend line. The averaged standard deviation of the Young's modulus amounts to ± 4.5 GPa and can be considered as high

compared to the determined variation range. The process parameter sets marked in red were therefore selected for the further steps, since they have the lowest standard deviation compared to neighboring values and are almost equidistantly distributed in the entire variation range. It should be positively emphasized that especially for process parameter sets with lower Young's moduli (#1, #4, #6) a low standard deviation between ± 1.4 and 2.4 GPa could be achieved. This is necessary to reliably increase resilience at the critical component location and to shift stresses toward stiffer component regions. However, in the region of higher Young's moduli (#12, #13, #14), standard deviations between ± 4.3 and 5.4 GPa were encountered, resulting in less reliable stiffening of the lower stressed component regions.

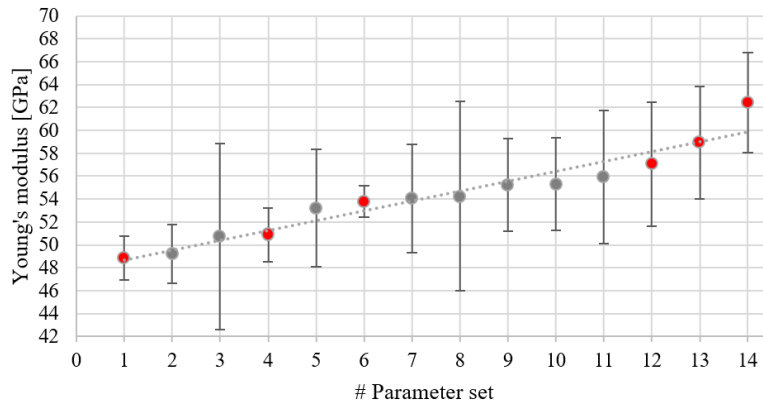


Figure 5: Young's modulus from tensile tests of specimens numbered according to parameter set

Figure 6 illustrates the Young's moduli compared to the volumetric energy density of the process parameter sets. The measured Young's moduli and the corresponding process parameter sets are shown in table 3. The comparatively high Young's moduli of the parameter sets with lower volumetric energy density result from the typically high cooling rates of smaller melt baths. High cooling rates, in turn, lead to fine microstructures, which cause increased dislocation resistance at the grain boundaries and thus exhibit higher strength properties. At higher volumetric energy densities, on the other hand, the melt pools are more extensive and thus have larger areas of thermal influence, which lowers the cooling rates. The increased cooling times increase the grain size and the number of grain boundaries, thus reducing the dislocation resistance. An analysis of the grain growth direction or grain size to quantify the microstructure was not carried out.

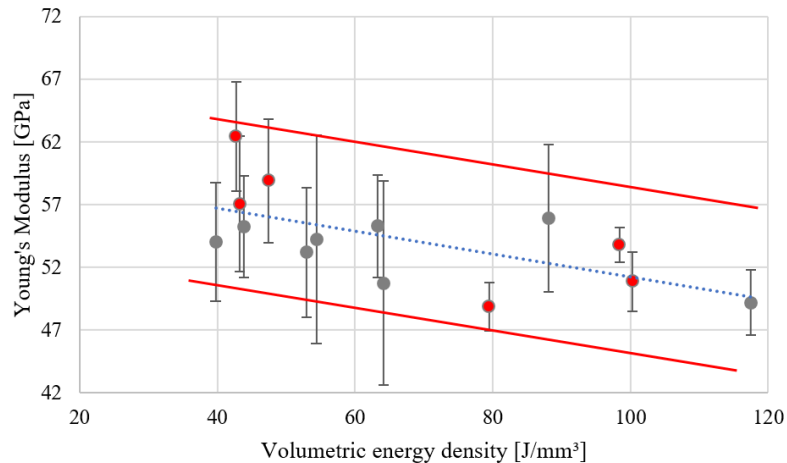


Figure 6: Young's moduli plotted against the volumetric energy density of the investigated process parameter sets

Table 3: Process parameter sets with the associated volume energy densities in ascending order of the measured Young's moduli

#	Laser power [W]	Scan speed [mm/s]	Hatch distance [mm]	Volumetric energy density [J/mm ³]	Youngs Modulus [GPa]
1	310	1000	0,13	79,49	48,9 ± 1,9
2	370	1500	0,07	117,46	49,2 ± 2,6
3	250	1000	0,13	64,10	50,7 ± 8,1
4	310	1500	0,19	100,27	50,9 ± 2,4
5	310	1500	0,13	52,99	53,2 ± 5,2
6	310	1500	0,07	98,41	53,9 ± 1,4
7	310	2000	0,13	39,74	54,0 ± 4,7
8	310	1000	0,19	54,39	54,2 ± 8,3
9	250	1000	0,19	43,86	55,3 ± 4,0
10	370	1500	0,13	63,25	55,3 ± 4,1
11	370	2000	0,07	88,10	55,9 ± 5,8
12	370	1500	0,19	43,27	57,1 ± 5,4
13	370	2000	0,13	47,44	58,9 ± 4,9
14	250	1500	0,13	42,74	62,4 ± 4,3

The selected process parameter sets are now used as a basis for the grading process with their corresponding Young's moduli. As a further constraint, the voxel size is set to 5 mm in order to counteract the thermal influence range of the different process parameter sets. The selection of the voxel size has to take into account that a too large edge length limits the optimization space, since, related to the dimensions of the geometry to be graded, too few gradations can be made over the components cross-section. If the voxels are chosen too small, there is a possibility that the thermal influence zone of process parameters with high volumetric energy density will influence the microstructure of areas that are to be manufactured with a low energy input. This lowers the cooling rate and thus tends to raise the Young's modulus due to the formation of increased grain growth. A certain influence by neighboring voxels cannot be avoided and is even desired to a certain extent in order to create transition areas between the voxels that prevent stiffness steps within the component.

Figure 7 shows the results of the finite element analysis in the context of grading the specimen with bore. After the FE analysis of the component was performed with homogeneous material parameters, the mesh was iteratively refined at the highly stressed locations in the edge regions of the hole, as shown in Figure 7. After three iterations with graded material properties, the maximum stress occurring in the critical location could no longer be reduced and the grading process was terminated. The analysis shows that the maximum stress at the critical point could be reduced by 16%.

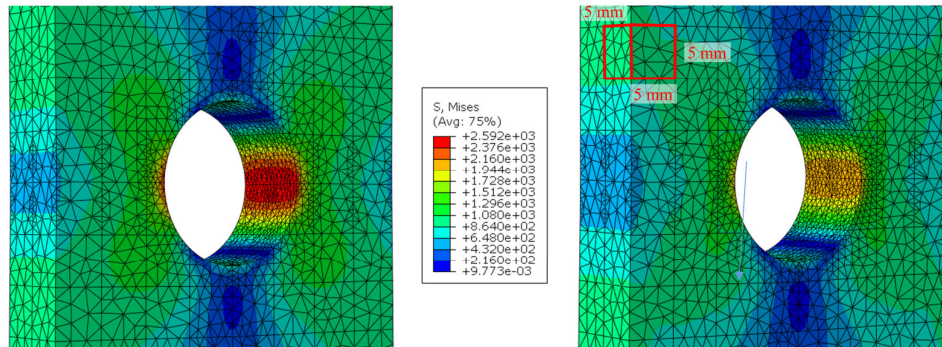


Figure 7: Results of finite element analysis on specimens with homogeneous (left) and graded (right) material properties, each voxel has an edge length of 5 mm as marked in red

Table 4 gives an overview of the resulting grading of the specimen geometry. It can be seen that the highest Young's modulus has been assigned in the region of clamping. As expected, the lowest Young's modulus was selected in the region of maximum stress. The stress magnification at the hole is so high compared to surrounding areas that material 5 has not been assigned due to the grading tool's assignment strategy. A smaller voxel size would provide a remedy and allow a more graded assignment, since the average stress within a voxel is crucial for the material assignment. In contrast, however, a smaller voxel size would have resulted in material 6 being assigned to a smaller volume, since the highest stress occurs only at the outer edge of the bore, thus raising the average stress only in the outermost voxel. The choice of relatively large voxels ensures that the heat-affected zones of the voxels with higher volumetric energy densities cannot have too great an influence on the voxels with material 6. As expected, materials 2, 3 and 4 were assigned to the remaining areas of the sample geometry according to the finite element analysis.

Table 4: Assignment of the graded Young's moduli based on the results of the grading tool

Material	Young's Module [GPa]	# Parameter set
1	62,4 ± 4,3	14
2	58,9 ± 4,9	13
3	57,1 ± 5,4	12
4	53,9 ± 1,4	6
5	50,9 ± 2,4	4
6	48,9 ± 1,9	1

In accordance to the material allocation shown above, graded specimens are now manufactured and subsequently tested in the tensile test and compared with specimens manufactured with the standard parameter set. Figure 8 shows the results of one graded and one homogeneous specimen each in the stress-strain diagram as representative of all tested specimens. The indicated stress σ is the technical stress, related to the cross-section at the critical point ($24 \times 10 \text{ mm}^2$). However, due to the brittle material behavior, the engineering stress is almost identical to the true stress, since almost no necking occurs in the region before the specimen failure. For this reason, the yield strength is given as $R_{p0.1}$, which corresponds to a permanent deformation of 0.1% compared to the initial length.

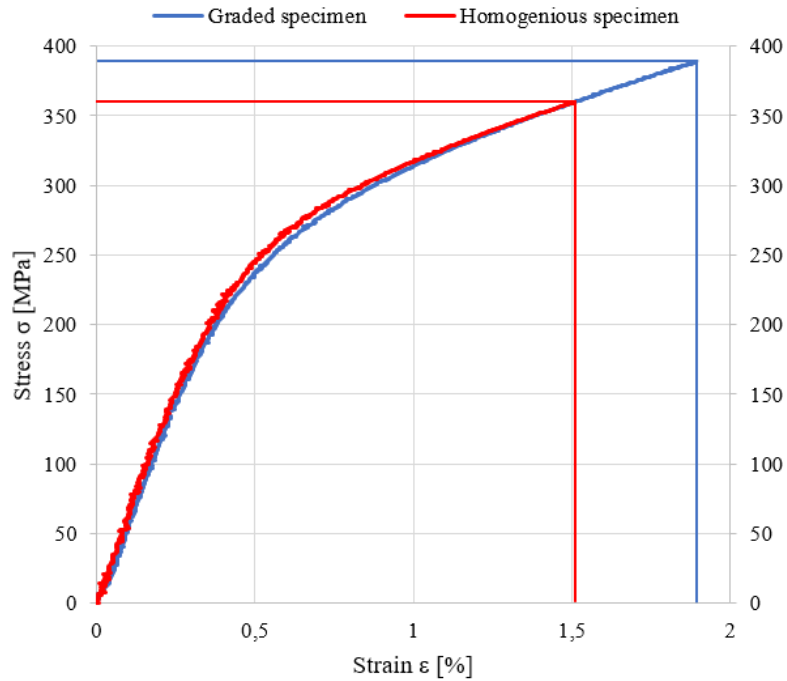


Figure 8: Stress-strain diagram from tensile tests on two representative specimens with bore manufactured using homogeneous and graded process parameters

Table 5 shows the averaged values for the characteristic points of the stress-strain curves. Eight homogeneous and eight graded specimens each were evaluated. The global behavior of the investigated specimens in the linear-elastic range is almost identical despite the different control of the manufacturing process, as shown both by the parallelism of the curves at the beginning in the stress-strain diagram and by the determined specimen-specific Young's Moduli in table 3. The first difference between the two curves shown in Figure 8 appears at the end of the yield strength $R_{p0.1}$, where the graded specimen enters the plastic region slightly earlier. However, since the difference between the yield strengths of homogeneous and graded specimens is less than their standard deviation, no significant difference in the transition from the elastic to the plastic zone can be stated here. After small deviations of the two specimens at the beginning of the plastic zone, the curves converge again until the failure of the homogeneous specimen. On average, the graded specimens show a 5% increase in tensile strength compared to the homogeneous specimens. This may be due to the fact that the additive processed material AlSi10Mg shows a strongly brittle material behavior. When cracking starts, the weakening of the structure leads to abrupt failure of the component. By slightly increasing the elasticity at the critical point of the component, the start of the crack can be delayed slightly due to the reduced local stress and thus leads to an increased tensile strength. In addition to the increased tensile strength, the maximum elongation of the graded specimen was increased by 17%. No difference was noticeable in the fracture locations and patterns of the homogeneous and graded specimens.

Table 5: Averaged results of tensile tests on graded and homogeneous specimens with bore

	Graded specimen	Homogenous specimen
Specimen-specific Young's Modulus [GPa]	62.8 ± 2.5	64.1 ± 3.9
Yield strength R _{p0.1} [MPa]	232.8 ± 6.7	235.6 ± 6.6
Tensile strength R _m [MPa]	377.6 ± 13.6	358.7 ± 12.0
Max. strain ε [%]	1.5 ± 0.2	1,8 ± 0,2

The global component behavior of the graded specimens deviates only marginally from the homogeneous specimens and therefore the investigated approach promises an improvement in the mechanical load-bearing capacity of additively manufactured components without the need to macroscopically adjust the geometry. Of course, the increase in tensile strength by 5% is not always in proportion to the effort involved, but this study shows that the performance of additively manufactured components can be increased in principle by influencing the manufacturing process in a targeted manner.

Summary and Outlook

In this work, a process window for varying the Young's modulus was first determined using a full-factorial experimental design. For this purpose, the density of the components that could be produced with the 27 sets of process parameters was first determined. Tensile specimens were then fabricated and subtractively post-processed to determine the mechanical properties of the process parameter sets. A variation of the Young's modulus in the range of 48.9 ± 1.9 to 62.4 ± 8.6 GPa could be achieved. In this range, 6 parameter sets were selected with an equidistant distribution in between the identified limits. Subsequently, a plate with a bore under tensile load was selected as test geometry and analyzed via finite element analysis with regard to the maximum stress occurring. Using the grading tool, the test geometry was divided into voxels and a load-adjusted grading of the Young's modulus was applied according to the stresses occurring. Through the grading, a reduction of the maximum stress of 16% on the inside of the bore could be determined in the FE analysis. In the subsequent examination of the manufactured test geometry in the tensile test, the tensile strength of the graded specimens was increased by 5% compared to the homogeneous specimens. This is presumably due to the fact that the ductility at the critical point could be increased locally, which delayed the cracking of the specimen. Despite the grading of the elastic modulus over the entire test geometry, the global behavior in the linear-elastic region was not significantly influenced. Due to the increased tensile strength, the maximum elongation of the specimen could be increased by about 17%.

In future investigations of this approach, the effect of anisotropy as related to the build direction must be considered. In addition, the cooling rates for the manufacturing of a specific microstructure must be determined. Further adaptation of the manufacturing strategy to meet the targeted cooling rates, for example by pausing between the individual layers, can also increase the potential of this approach.

References

- [1] J. Reichwein, S. Vogel, S. Schork, and E. Kirchner, "On the Applicability of Agile Development Methods to Design for Additive Manufacturing," *Procedia CIRP*, vol. 91, pp. 653–658, 2020, doi: 10.1016/j.procir.2020.03.112.
- [2] T. Wohlers, R.I. Campbell, O. Diegel, J. Kowen, and N. Mostow, *Wohlers report 2021: 3D printing and additive manufacturing*. Fort Collins, Colorado: Wohlers Associates, 2021.
- [3] J. Zhu, H. Zhou, C. Wang, L. Zhou, S. Yuan, and W. Zhang, "A review of topology optimization for additive manufacturing: Status and challenges," *Chinese Journal of Aeronautics*, no. 34, pp. 91–110, 2021, doi: 10.1016/j.cja.2020.09.020.
- [4] E. Brandl, U. Heckenberger, V. Holzinger, and D. Buchbinder, "Additive manufactured AlSi10Mg samples using Selective Laser Melting (SLM): Microstructure, high cycle fatigue, and fracture behavior," *Materials & Design*, vol. 34, pp. 159–169, 2012, doi: 10.1016/j.matdes.2011.07.067.
- [5] H. Merschroth, M. Kniepkamp, and M. Weigold, "Predicting and Controlling the Thermal Part History in Powder Bed Fusion Using Neural Networks," in *Proceedings of the 30th Annual International Solid Freeform Fabrication Symposium*, 2021, pp. 161–171.
- [6] M. E. Kniepkamp, *Methode zur bauteilindividuellen Prozesssteuerung beim selektiven Laserschmelzen*, 1st ed. Düren: Shaker Verlag, 2020.
- [7] A. H. Maamoun, Y. F. Xue, M. A. Elbestawi, and S. C. Veldhuis, "The Effect of Selective Laser Melting Process Parameters on the Microstructure and Mechanical Properties of Al6061 and AlSi10Mg Alloys," *Materials (Basel, Switzerland)*, vol. 12, no. 1, 2018, doi: 10.3390/ma12010012.
- [8] J. P. Oliveira, T. G. Santos, and R. M. Miranda, "Revisiting fundamental welding concepts to improve additive manufacturing: From theory to practice," in *Progress in Materials Science*, 2020, p. 100590.
- [9] Y. Parikh and M. Kuttolamadom, "Selective Laser Melting of Stainless Steel 316L for Mechanical Property-Gradation," in *Volume 1: Additive Manufacturing; Advanced Materials Manufacturing; Biomanufacturing; Life Cycle Engineering; Manufacturing Equipment and Automation*, Virtual, Online, 2021.
- [10] V. A. Popovich, E. V. Borisov, A. A. Popovich, V. Sufiiarov, D. V. Masaylo, and L. Alzina, "Functionally graded Inconel 718 processed by additive manufacturing: Crystallographic texture, anisotropy of microstructure and mechanical properties," *Materials & Design*, vol. 114, pp. 441–449, 2017, doi: 10.1016/j.matdes.2016.10.075.
- [11] B. Attard, S. Cruchley, C. Beetz, M. Megahed, Y. L. Chiu, and M. M. Attallah, "Microstructural control during laser powder fusion to create graded microstructure Ni-superalloy components," *Additive Manufacturing*, vol. 36, p. 101432, 2020, doi: 10.1016/j.addma.2020.101432.
- [12] R. Bürgel, *Festigkeitslehre und Werkstoffmechanik*. Wiesbaden: Vieweg+Teubner Verlag, 2005.
- [13] J. Geis, H. Merschroth, T. Sommer, E. Kirchner, and M. Weigold, "Konstruktive Potentiale einer Mikrostrukturgradierung von topologieoptimierten L-PBF-Bauteilen," in *DS III: Proceedings of the 32nd Symposium Design for X*, 27 and Sep. 2021.

- [14] M. Giovagnoli, G. Silvi, M. Merlin, and M. T. Di Giovanni, "Optimisation of process parameters for an additively manufactured AlSi10Mg alloy: Limitations of the energy density-based approach on porosity and mechanical properties estimation," *Materials Science and Engineering: A*, vol. 802, p. 140613, 2021, doi: 10.1016/j.msea.2020.140613.
- [15] R. C. Hibbeler, *Technische Mechanik 2 Festigkeitslehre: Lehr- und Übungsbuch*, 8th ed. München: Pearson Studium, 2013.
- [16] EOS GmbH, *EOS Aluminum AlSi10Mg Material Data Sheet*. [Online]. Available: www.eos.info/03_system-related-assets/material-related-contents/metal-materials-and-examples/metal-material-datasheet/aluminium/material_datasheet_eos_aluminium-alsi10mg_en_web.pdf (accessed: Jun. 19 2022).